Earth and Planetary Science Letters 367 (2013) 71–81

Contents lists available at SciVerse ScienceDirect

Earth and Planetary Science Letters

journal homepage: www.elsevier.com/locate/epsl

P and SH velocity structure in the upper mantle beneath Northeast China: Evidence for a stagnant slab in hydrous mantle transition zone

Juan Li [a,*], Xin Wang [a], Xiujiao Wang [a], David A. Yuen [b,c]

[a] Key Laboratory of the Earth's Deep Interior, Institute of Geology and Geophysics, Chinese Academy of Sciences, 100029 Beijing, China
[b] Department of Earth Sciences, University of Minnesota, Minneapolis, MN 55455, USA
[c] School of Environment Sciences, China University of Geosciences, 430074 Wuhan, China

ARTICLE INFO

Article history:
Received 25 October 2012
Received in revised form
19 February 2013
Accepted 23 February 2013
Editor: P. Shearer
Available online 21 March 2013

Keywords:
mantle transition zone structure
waveform modeling
seismic wave speed
northwestern Pacific subduction zone
stagnant slab
water bearing mantle transition zone

ABSTRACT

Using high-dense regional body waves for three deep earthquakes that occurred around Russia–China border, we investigate both S and P wave velocity structures in the mantle transition zone beneath Northeast China and northern part of North China Craton, where the northwestern Pacific plate is imaged to subhorizontally lie above the 660-km discontinuity. We observe an increasing trend of S–P travel time residuals along the epicentral distance within a distance range of 11–16.5°, indicating a velocity anomaly in MTZ. We seek the simplest model that explains the observed broadband waveforms and relative travel times of triplication for a confined azimuth sector. Both SH and P data suggest a $\sim 140 \pm 20$ km high velocity layer lying above a slightly depressed and broad 660-km discontinuity. Shear velocity reduction of ~2.5% in the deeper part of the transition zone is required to compensate for the significantly large relative time between AB and CD triplicate branches and the increased trending of S–P travel time residuals as well. The MTZ, as a whole, is featured by low shear velocity and high V_p/V_s ratio. A water-rich mantle transition zone with 0.2–0.4 wt% of H_2O may account for the discrepancy between the observed V_p and V_s velocity structures. Our result supports the scenario of a viscosity-dominated stagnant slab with an increased thickness of ~140 km, which was caused by the large viscosity contrast between the lower and upper mantles. The addition of water and eastward trench retreat might facilitate stagnation of the subducting Pacific slab beneath Northeast China.

1. Introduction

Seismic structure of the mantle transition zone (MTZ), a region connecting the upper and lower mantles, is important for better understanding of how mantle works as a thermal–chemical engine. The interaction between the upper mantle discontinuities and the subducting lithosphere results in a heterogeneous MTZ. A depressed 660-km discontinuity (hereafter referred to as the 660) is generally expected in the cold subduction regions due to the negative Clapeyron slope of the postspinel transformation (e.g. Ito and Takahashi, 1989). The undulation of the discontinuities can be regarded as a sensitive thermometer in the Earth's deep mantle.

One ideal place to study the interaction between a subducting slab and the 660 is northeast China (Fig. 1), where the subducted Pacific slab seems to be lying sub-horizontally in the MTZ (Li and van der Hilst, 2010; Huang and Zhao, 2006; Fukao et al., 2009). However, a slab directly penetrating into the lower mantle is also proposed beneath Japan by global P-wave tomography (Bijwaard et al., 1998). Substantial difference in the stagnant slab images has been detected by a joint bulk-sound and shear wave travel-time inversion (Gorbatov and Kennett, 2003). Recent study in quantifying uncertainty in travel-time tomography reveals that the root mean square velocity perturbations for a bunch of acceptable models compatible with the same travel time dataset can vary from 0.3% to 1.3% in the upper mantle (de Wit et al., 2012), which might reflect the intrinsic problems of nonuniqueness of images and poor depth resolution in seismic tomography.

An alternative seismic approach for constraining topography of the discontinuities and velocity structure is waveform modeling. Regional triplication waveform has been modeled effectively in detecting anomalies associated with subduction process. An ultralow velocity zone atop the 410-km discontinuity has been mapped beneath northwestern United States (Song et al., 2004), which might be caused by partial melting of a prior subduction of Farallon plate. A high velocity layer beneath northwestern Pacific subduction zone has been suggested by various P or S triplication waveform modeling (Tajima and Grand, 1995; Tajima et al., 2009; Wang and Niu, 2010; Wang et al., 2006; Wang and Chen, 2009; Ye et al., 2011). However, partly due to the limitation of stations and large lateral variation of velocity, there is considerable discrepancy

* Corresponding author. Tel.: +86 10 82998446.
E-mail address: juanli@mail.iggcas.ac.cn (J. Li).

0012-821X/$ - see front matter © 2013 Elsevier B.V. All rights reserved.
http://dx.doi.org/10.1016/j.epsl.2013.02.026

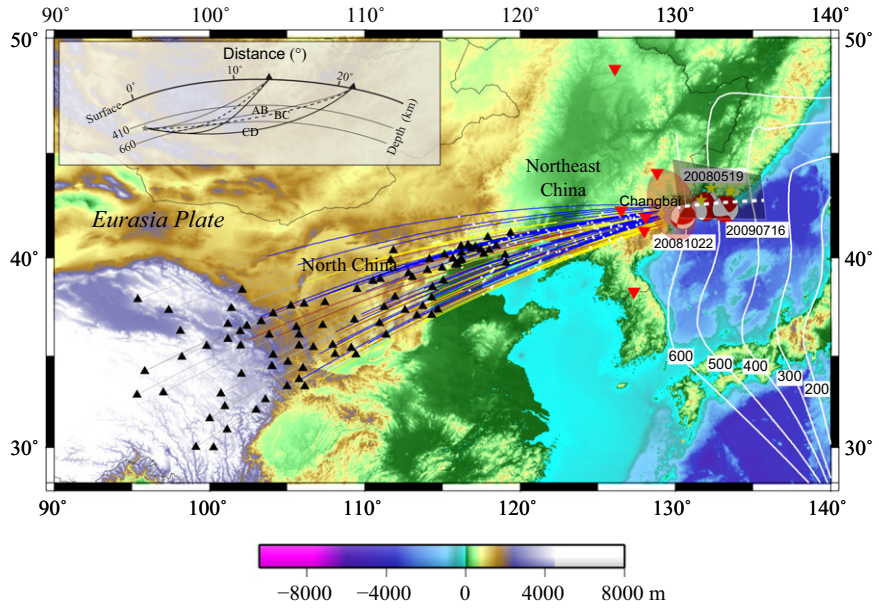

Fig. 1. Map showing location of deep earthquakes and regional seismic stations used in this study. Focal mechanisms for three events used in triplication waveform modeling are shown with red beach balls. Regional seismic stations are shown by black triangles. Blue, yellow and brown lines bounded by two sections of gray lines highlight portions of the ray traveling below the 660 for events 20080519, 20090716 and 20081022, respectively. White dots are turning locations of transversal CD phases calculated for the iasp91 model. The Wadati–Benioff zone is indicated by white solid lines. The yellow stars represent other deep events used in the travel-time analysis. Red inverted triangles indicate the Cenozoic active volcanoes, and the data are from www.ngdc.noaa.gov. The orange oval shows location of the 660 with depression ~30 km reported by Li and Yuan (2003); the black quadrangle shadow next to it corresponds to region with 660 undulation mapped by source-sided S-to-P converted wave study (Li et al., 2008), and the dashed white line indicates the profile of the constrained 660 topography. The upper inset is a schematic diagram of triplication, which includes AB branch—the direct wave propagating above the discontinuity, BC branch—the wide-angle reflection off the discontinuity, and CD branch—the waves diving below the discontinuity. (For interpretation of the references to color in this figure legend, the reader is referred to the web version of this article.)

in MTZ structure, yielding ambiguous interpretations about the structure and composition of the deep upper mantle and the underlying dynamic process (e.g. Li and Yuan., 2003; Li et al., 2008).

In the current study, we report findings based on broadband waveforms of both vertical (P) and horizontally polarized shear waves (SH) for three recent deep earthquakes recorded by the dense Chinese Regional Seismic Network. We use exactly the same station-receiver geometry for both P and SH waves, and investigate the fine-scale shear and compressional velocity structure. We expand and refine our previous results of shear wave velocity (Ye et al., 2011) obtained from a single earthquake, investigate both S–P travel-time residuals and triplication waveforms, and show new and confirmable evidence for shear velocity anomaly in the deeper part of the MTZ. We briefly introduce the method and data in Section 2; analyze the S–P travel time residuals and apply the regional triplication waveform modeling to get fine scale structure for both V_p and V_s in Sections 3 and 4 respectively; we will finally constrain thermal or/and compositional anomaly from the joint P and SH wave velocity study, and discuss the implication on dynamic subduction process beneath northeast China.

2. Method and data

Seismic waveform modeling of regional triplication phases is applied to investigate velocity structure in the MTZ. The triplication waveforms include three sets of arrivals: the waves propagating above the discontinuity (AB), the wide-angle reflection of the discontinuity (BC) and the waves diving below the discontinuity (CD) (inset in Fig. 1). Since ray paths of the three phases are very close to each other in the crust and uppermost mantles, the relative time interval and amplitude between those arrivals are primarily sensitive to velocity structure near the discontinuity. For example, the termination distance of AB phase (i.e. location of cusp-B) is sensitive to the velocity gradient above the discontinuity; the move out of CD phase (i.e. location of cusp-C) is sensitive to the velocity gradient below the discontinuity; and the travel time difference between AB and CD phases mainly reflects velocity contrast above and below the discontinuity.

We used three-component broadband seismic waveforms collected from dense regional seismic networks in China which had been installed in 2007 (Zheng et al., 2010). To avoid effect resulted from shallow upper mantle discontinuities, three moderate-sized earthquakes with epicentral depth greater than 410 km were selected (Table 1). All of them occurred in the Japan sea near the border of Russia and China (Fig. 1), and displayed simple source time functions (STFs) which are favorable for mantle structure investigation. For convenience, we named them as events 20080519, 20081022 and 20090716.

Event 20080519 with Mw 5.9 has the highest signal-to-noise ratio for both P and S waveforms in regional distances. In addition, this event produced enough teleseismic records with high SNR for focal depth determination. We handpicked pP and P phases from 330 teleseismic records with good azimuth coverage, and redetermined the epicentral depth to be 519 ± 3 km by minimizing the residual of differential time of pP–P relative to iasp91 model. The SNR of teleseismic records for the other two events is low, and we adopted the epicentral depth from PDE catalog (Table 1).

We confine distribution of stations to a narrow azimuthal range of 255–272° based on previous studies (Wang and Niu, 2010; Ye et al., 2011) to reduce the lateral velocity variation. The direction of constructed seismic fan-shot is roughly perpendicular to the strike of the Wadati–Benioff zone around latitude 42–43°N (Fig. 1). It should be noted that we select and keep those waveforms with both P and S triplication phases clearly identified for a simultaneous investigation of shear and compressional velocity structures. The turning points of the directed and refracted rays sample the MTZ extensively west of the Japan

Table 1
Information of earthquakes used in triplication waveform modeling.

Event ID	Origin	Time	Location		Magnitude	Depth		
			Lat. (deg.)	Lon.	(Mw)	PDE (km)	CMT	Used
20080519	19/05/2008	00:08:36.31	42.50	131.87	5.6	513	522	519[a]
20090716	16/07/2009	06:29:04.76	42.37	133.00	5.3	477	485	477
20081022	22/10/2008	16:18:36.40	41.99	131.32	4.7	573	–	558[b]

[a] Depth determined by minimizing residual differential times of pP–P relative to the iasp91 model.
[b] Depth and source mechanism are determined by the "cut and paste" method through local waveform modeling. Focal mechanism of event 20081022 applied here is strike=81, dip=40, and slip=138.

trench, and the exact same station-event geometries for P and S waves allow a tight constrain in both kinds of wave velocity near the 660 beneath the northwestern Pacific subduction zone.

3. Travel time anomalies associated with MTZ

Travel time of body waves along various paths offers the most direct information for velocity variations in the mantle (e.g. Molnar and Chen, 1984). We first applied an initial but direct travel time analysis for both S and P waves to get the first-order impression of existence of an anomaly structure associated with MTZ. We checked both horizontal components to make sure the polarities of signals are consistent with each other (Niu and Li, 2011; Li and Niu (2010)). We then removed the instrumental response and applied band-pass filters of 0.04–1 Hz and 0.04–0.5 Hz to vertical and transversal displacements, respectively. We measured first arrivals of S and P waves from vertical and transversal components for all available records in the regional distance. To quantify the effect of upper mantle anisotropy, we also handpicked first arrival time from radial components, and the arrival time difference between SH and SV is generally smaller than 0.2 s.

We noticed that two GSN stations – XAN (34.03°N, 108.92°E) and BJT (40.02°N, 116.17°E) – are located within the constructed fan-shape region. For a good calibration and comparison, we downloaded seismic waveforms from IRIS and epicentral information from EHB catalog for another three moderate deep earthquakes which occurred near the same region, and handpicked their arrival times (Fig. 1).

Fig. 2a shows P and S wave time residuals relative to model iasp91 for events 20080519, 20090716 and another three events. The SNR of vertical component of event 20081022 is low, and no first P arrivals can be clearly identified. A total of 95 and 88 records are retained for events 20080519 and 20090716, respectively. We analyzed those arrivals before the CD branch crossovers AB for the reason that the first arrival of AB phase for P and SH waves has almost identical ray paths through the MTZ. To minimize possible scatter due to differences in velocities beneath stations, we calculated S–P travel time residuals, which are the differences between the observed and calculated intervals between S wave and P wave arrival time (Fig. 2b).

The most obvious feature in these data is the enormous scatter in S time residuals, which characterizes almost all studies of S wave residuals. For distance shorter than 10°, the P time residuals are around 1.5 s, while the values of S wave are ~2–3 s, indicating contribution from the heterogeneity in the crust or shallow upper mantle. A systematical larger time residuals are observed for event 20090716 at shorter epicentral distances, which might be caused partly by the uncertainty of focal depth. Within distance range of 10–17°, the P travel time residuals range generally from −0.5 to 2 s with an average value of ~1 s. The residuals of S wave are much larger, ranging between 0.5 and 3.8 s (Fig. 2a). It has

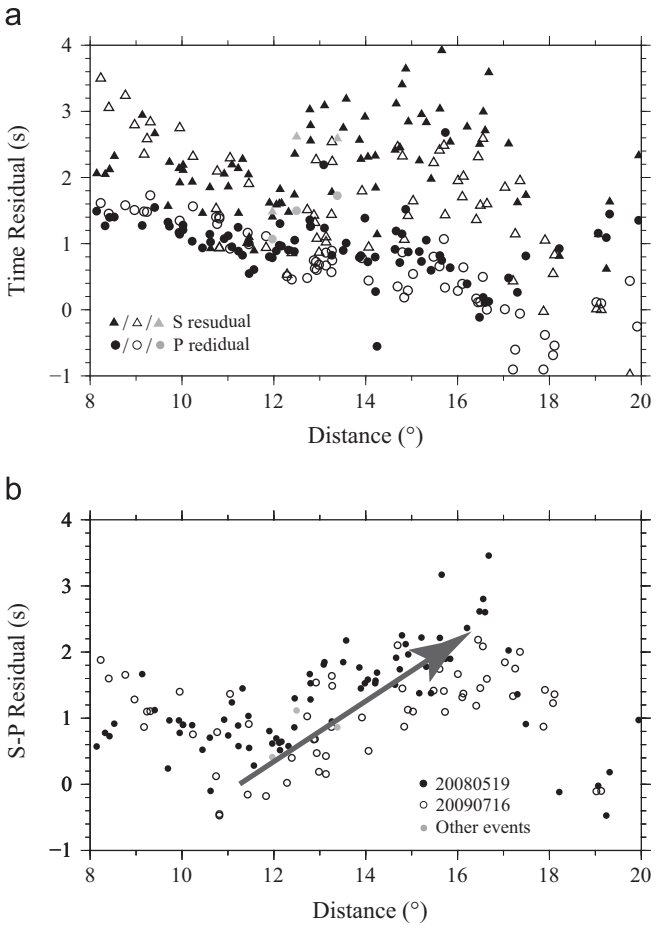

Fig. 2. P and S travel-time residuals (a) and S–P travel-time residuals (b) relative to the model iasp91 are shown with variation of epicentral distance. (a) Data for events 20080519 and 20090716 are handpicked from regional seismic networks, which are marked by solid and hollow symbols, respectively. Arrival times for two GSN stations of other deep events are marked by gray symbols. (b) Solid, hollow and gray dots indicate S–P travel-time residuals for events 20080519, 20090716, and other events, respectively. An increasing trend of S–P residuals can be obviously seen within the distance range of 11–16.5°.

been shown that even for the Pn and Sn waves, which travel thoroughly through the shallow upper mantle, the observed residual time beneath east China can be several seconds, and the station correction can be as large as ~2–3 s (Pei et al., 2007). Despite the large scattered data, however, there is an obvious increasing trend of S–P residuals (Fig. 2b) within epicentral distance of 11–16.5°. For event 20080519, the average value of S–P differential time residuals at distances $<11°$ is 0.7 s, and then it increases from ~0.3 s to a peak value of ~2.8 s at distance ~16.5°. Despite relatively low SNR, the S–P travel time residual of

event 20090716 shows the same increasing trend within epicentral distance of 11–17°.

In general, S–P travel time residuals are caused by the integrated velocity anomalies along ray paths from the source to the receiver. We notice that values of S–P residuals are closely related to the turning depth of rays. The deeper the turning depth is, the longer the ray travels through the MTZ. All S–P residuals larger than 2 s are from rays turning in the deeper MTZ. We thus infer that the increasing trend of S–P residual beyond 11° is caused by the anomaly structure in the MTZ: either the shear velocity is relatively low, or the P wave velocity is relatively faster, which will be further explored in regional triplication waveform modeling. Around epicentral distance ~16.5°, CD branch of triplication phase, which dives in the upper lower mantle, becomes the first arrival and terminates the increasing trend of S–P time residuals (Fig. 2b). We emphasize that in our study, the absolute travel time is not used to constrain the deep MTZ structure; however, the S–P residual analysis gives us a simple and effective way to detect seismic velocity structure anomaly associated with the deep upper mantle to the first order.

4. Triplication waveform modeling

Triplication waveform modeling has been widely applied to constrain mantle structure (e.g. Grand and Helmberger, 1984; Wang and Yao, 1991; Tajima and Grand 1995, 1998; Brudzinski and Chen, 2000, 2003; Song et al., 2004). Due to sporadic distribution of seismic instrumentations, most previous studies were based on individual seismogram analysis, which is hard to resolve the trade-off between the interface depth and velocity variation. With the rapidly increasing installation of broadband seismic stations, record section of seismogram as functions of epicentral distance within a limited azimuth range becomes much more useful and reliable for exploration of vertical deep structure (e.g. Wang and Niu, 2010; Ye et al., 2011). To illustrate how velocity variation affects aligned triplication waveforms, we show synthetic seismograms for a set of velocity models which are proposed to characterize deep structure at subducting tectonic settings (e.g. Tajima and Grand, 1998; Wang et al., 2006; Wang and Niu, 2010; Ye et al., 2011) in Section 1 of Supplementary material.

We emphasize that in the following regional triplication waveform modeling, we are trying to find the simplest model to match the general feature of the whole set of seismograms, for example, the move out of cusp-B, cusp-C and O point, the relative time and amplitude between AB and CD phases, rather than the absolute arrival times of triplicate phases. The major feature of triplication appeared in an aligned seismogram, instead of an individual waveform record, allows us to constrain the fine-scale velocity structure effectively and accurately.

The source mechanisms for events 20080519 and 20090716 are from Global CMT. The released seismic energy of event 20081022 with Mw 4.7 is small, and the double couple solution is from Li (2012), who applied the cut and paste (CAP) method (Zhu and Helmberger, 1996) to local stations for a simultaneous inversion of the depth and source mechanism (Table 1). A Gaussian wavelet is used to represent the source time function considering the simple teleseismic waveform.

To compensate the large P and S time residuals observed even at shorter distance as shown in Fig. 2a, which mainly result from the heterogeneity in the shallow Earth, we adopted a similar approach as Tajima and Grand (1998), and Wang and Chen (2009), by modifying the velocity structure above the 410 km after Fukao (1977). This greatly improved the consistency in absolute times at those distances. The velocities deeper than 410 km are further constrained by triplication waveform modeling.

4.1. Compressional velocity structure in deeper upper mantle

In the aligned vertical waveforms, we can clearly identify triplicate branches in a regional distance range of 11–30° for all events. For event 20080519 (Fig. 3a), AB phase starts to appear weaker at distance ~24° and becomes indiscernible around 25°. CD phase begins to appear at epicentral distance of 15°, and crosses over AB phase at ~18°, sampling the top of the lower mantle to depth of ~682 km. Despite relatively low SNR, seismic waveform of event 20090716 displays the same features. For example, AB branch can be clearly identified until at distance ~26° (Fig. 5a). CD phase begins to emerge at a distance about 15.5–16°, and crosses over the AB phase at an epicentral distance ~18.5° with sampling depth ~676 km.

The triplication of both events share three major features which cannot be explained by model iasp91. The most obvious one is that the disappearing distance of AB phase is much larger than the value predicted from iasp91. The predicted locations of cusp-B are 21.4° and 22.4° for the two events, which are much shorter than the observation. The second is that cusp-C appears at a greater epicentral distance than predictions of 12.1° and 12.8° from the iasp91 model. The third is that CD phase crosses over AB phase at a distance of 1.5–2° further than the reference values of 16.7° and 17.7°.

We obtained the best fitting model by searching models with velocity structures varied around the 660. The depth of the 660, the velocity jump across the discontinuity and the velocity gradient above and below the 660 are all judged to change through trial and error test based on synthetic waveform modeling. We calculated the coefficient of cross-correlation between the synthetic and observed waveforms to determine goodness of the fit.

The best fitting P velocity model is shown in Fig. 4a. The velocity of the upper part of the preferred model is almost identical to that of iasp91. However, a high velocity layer with thickness $\sim 140 \pm 20$ km (uncertainty estimation available in Supplementary material) lying above the 660 is required to match the long extension of cusp-B. The maximum fast velocity anomaly is 2.3% with an average value of ~1%. Another important feature is that the 660 seems to be a broad discontinuity with thickness $\sim 44 \pm 6$ km (see Supplementary material for uncertainty estimation), instead of a sharp velocity boundary (Fig. 4a).

4.2. Shear velocity structure in deeper upper mantle

The SNR of SH records is even higher than that of P components, and SH triplication is clearly identified in the aligned seismogram. For event 20080519 (Fig. 3b), AB branch extends to as far as 25°; CD branch begins to emerge at distance ~13.0°, crossing over the AB phase at ~16.1°, and samples the top of lower mantle to a depth of 779 km at 25°. In particular, we observed an obvious broadened BOD zone with significantly delayed AB wave after distance ~18° (Fig. 3b). The triplication for the other two events shows a further appearance of cusp-C, an extraordinary long extension of cusp-B, a shift of O point, and especially, a similar striking feature of a broadened BOD zone (Fig. 5b and c).

As in the compressional velocity structure modeling, a very gentle velocity gradient just above the 660 is required to explain the extension of AB branch to a distance ~25° in contrast to ~20° predicted by iasp91. A depressed 660 will result in an extension of AB branch; however, it will delay the CD branch in contrast to our observation. To explain the striking features of the observed broadened BOD zone, we need a low velocity layer at least in the deeper part of the MTZ (> 477 km) considering the shallowest depth of the events selected. It should be noted that the velocity structure shallower than that value is obtained mainly from the

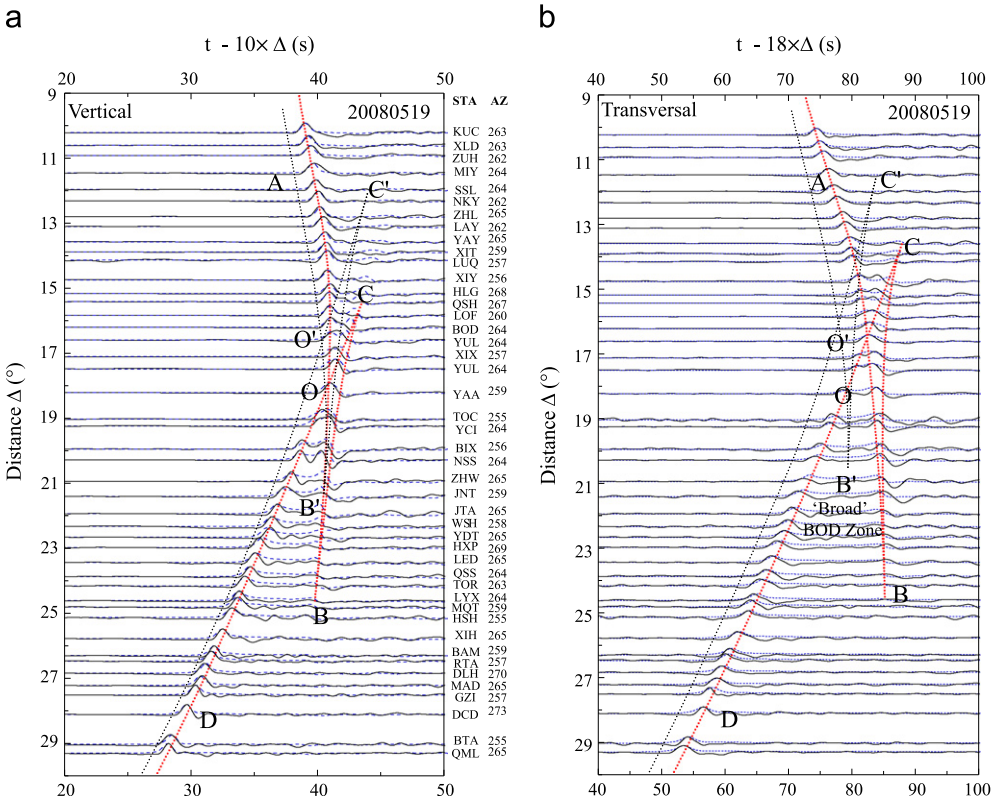

Fig. 3. Comparison of the observed (black solid line) and synthetic (blue dashed line) vertical and transversal waveforms computed from our preferred P and S velocity models for event 20080519. Black and red dotted lines are theoretical travel times based on iasp91 and preferred models calculated from Taup (Buland and Chapman, 1983), respectively. Observed seismograms were aligned with the synthetic one at the peak arrivals. Most of the absolute time corrections are smaller than 1 s, and for distance range 19–22°, the time correction is ~2 s, which might be related to the local structure beneath stations. Code and azimuth angle of each station are denoted on the right side of the vertical component. (For interpretation of the references to color in this figure legend, the reader is referred to the web version of this article.)

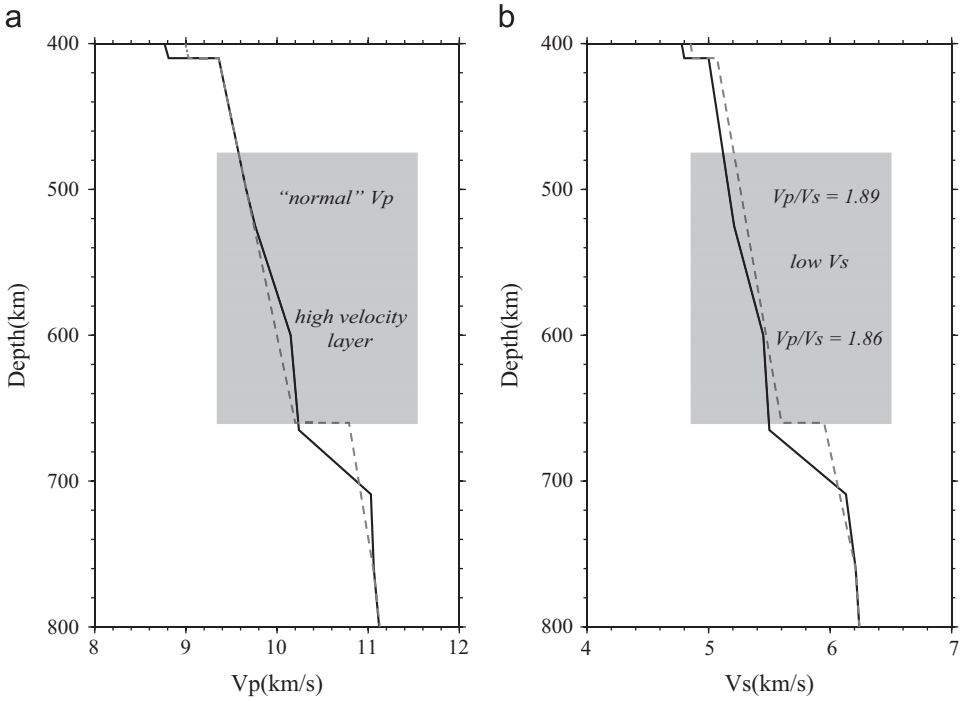

Fig. 4. Best-fitting compressional (a) and shear velocity (b) models around the 660-km discontinuity. The thin lines mark the reference model iasp91 for comparison. The gray square marks the region where the velocity structure can be constrained well by triplication waveform modeling. Uncertainties for depth of the 660, thickness of the high velocity layer above the 660, and the thickness of the broad 660 are available in the Supplementary material.

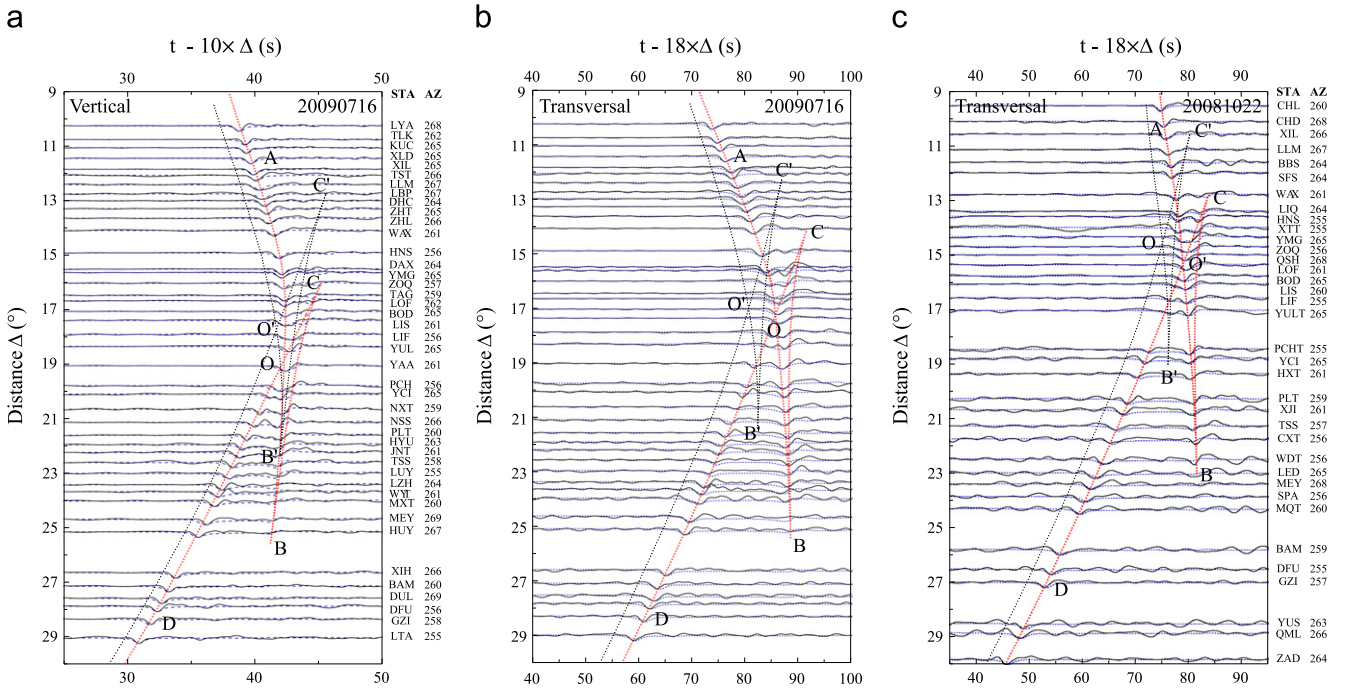

Fig. 5. Comparison of the observed (black solid line) and synthetic (blue dashed line) waveforms for events 20090716 ((a) and (b)) and 20081022 (c). Only transversal components are calculated and compared due to the low SNR of vertical component for event 20081022. (For interpretation of the references to color in this figure legend, the reader is referred to the web version of this article.)

travel time fitting, but not the triplication waveform modeling, and thus is less well constrained.

Consistent with P velocity structure, our preferred shear velocity model also shows the presence of a high velocity (~2%) anomaly with thickness $\sim 140 \pm 20$ km lying above the little depressed 660 (Fig. 4b). A broad 660-km discontinuity with thickness $\sim 44 \pm 6$ km is required to explain the later appearance of CD phase. The most intriguing feature is that, in contrast to the "normal" P velocity in the MTZ, the S velocity in the MTZ is rather low relative to iasp91 as a whole. Such feature casts significant constraint on the composition and thermal anomaly in the deeper MTZ which will be discussed in the following sections.

5. Discussion and interpretations

We simultaneously investigated P and S wave velocities in the deep MTZ beneath northeast China and northern North China Craton by triplication waveform modeling from three deep earthquakes. Several consistent prominent features have been detected in both P and S wave velocity structures. Uncertainty estimation of the key values associated with the structure, e.g. thickness of the high velocity layer, thickness of the broad 660, and velocity variation can be found in Section 2 of Supplementary material.

We see some mismatch between the synthetic and observed waveforms. Due to the nonuniqueness of the inversion problem, we could not rule out possibility of a better resolved model; however, the striking features in the records, like extended AB branch, shortened CD branch and "broad BOD", are well captured by the preferred models. We argue that lateral velocity heterogeneity might contribute to this inconsistency of the waveforms.

We further estimated effects of 3D velocity structure as imaged by seismic tomography on the relative travel time between the triplicate phases. We assumed a 2D raypath and counted the cumulative travel time anomalies caused by the structure (Li et al., 2008). We used P wave velocity model of Fukao et al. (2001) and an S wave velocity model converted from the P model with a scaling relationship of $\delta \ln V_s / \delta \ln V_p = 1.6$ (Karato and Karki, 2001). The absolute travel time correction for triplicate P wave is generally ~ -1 s. For example, the AB and CD phase travel time corrections between event 20080519 and station BU.LAY (lon: 114.98°, lat: 39.51°) are -0.9 s and -1.1 s, respectively. The time correction for S phase is a little larger with values ~ -1.6 s and -1.9 s. The correction for different travel time between AB and CD phases for P and S type waves, however, is generally trivial, usually < 0.3 s, which is smaller than the assumed misfit threshold in uncertain estimation for preferred models (Supplementary material).

In the following sections, we compare our results with previous typical models, and then show how the resolved P and S wave velocity structures might give some clues to compositional and/or thermal anomaly identification and for a good understanding of the dynamic subduction process beneath northeast China as well.

5.1. Comparison with previous typical models

Regional P waveform modeling by Tajima and Grand (1995) and the following series of work (Tajima and Grand, 1998; Tajima and Nakagawa, 2006) are among the earliest systematic studies on MTZ structure beneath northwestern Pacific subduction zone. A V_P model named as "M3.11" (e.g. Tajima and Grand, 1998) was proposed to represent structure of the upper mantle beneath northwestern Japanese subduction zone and the southern Kuriles. Model M3.11 is characterized by a 30-km depressed 660 and a high velocity anomaly in the deeper part of the MTZ (inset of Fig. 6). A low gradient high velocity layer is invoked to match the long extension of AB phase observed from individual records at larger distance, which could be more readily seen from our aligned seismograms (Fig. 3). However, the super long extension of cusp-B, a shorter emerging distance of CD phase and 1.5° down-shift of O point for event 20080519 with the highest SNR seem to be inconsistent with the observation (Fig. 6a). We noticed that the individual record used to derive their model is mainly confined to distance $> 18°$ due to the spotty distribution of permanent stations in the 1990s, and thus the structure just below the 660 could not

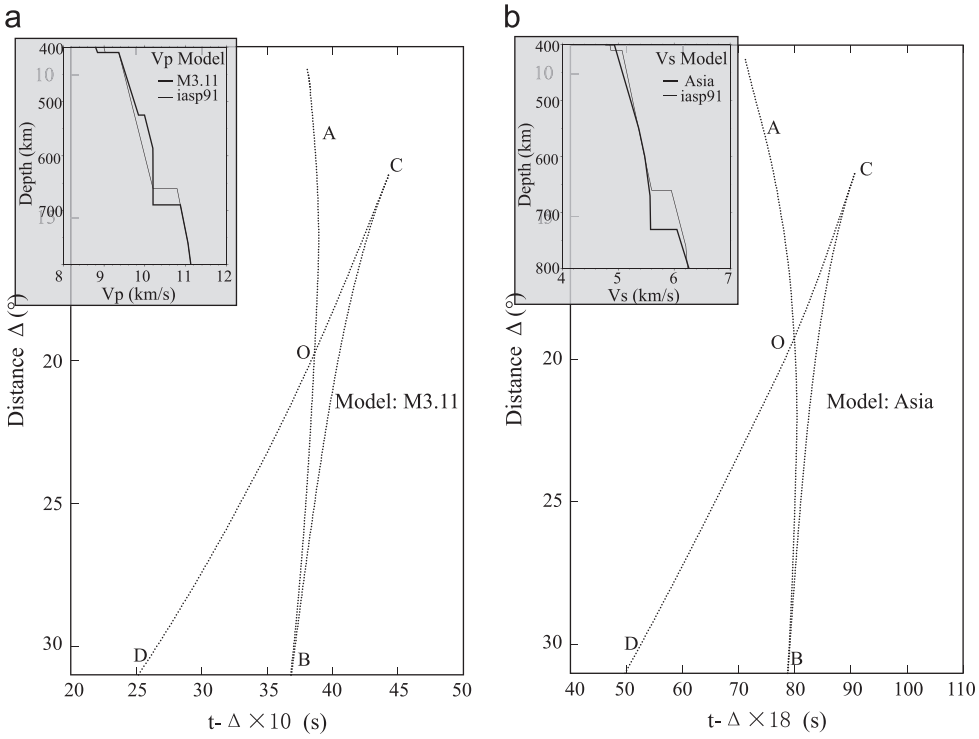

Fig. 6. Comparison of previous typical (a) P and (b) S velocity models. P velocity model "M3.11" (Tajima and Grand, 1998) is characterized by a 30-km depressed 660 and a high velocity layer above the 660. The 660 was depressed to as deep as 730 km in the S velocity model "Asia" (Wang et al., 2006). Travel time curves calculated for the two models for event 20080519 are represented by the dotted lines.

be constrained well. This may also explain why their synthetic waveforms match the observed vertical wiggles at further distance much better than at shorter distance.

Wang et al. (2006) applied SH waveform modeling to northeast Asia and obtained shear velocity structure "Asia" from two deep earthquakes using a large-aperture seismic array. One of the most important inferences of their results is that a lateral variation of shear velocity is not significant throughout eastern Asia. A significant depression of the 660 to 730 km was introduced, resulting in a further terminal distance of AB phase at 32° as shown in Fig. 6b. The location of O point is shifted 3° further also. Especially, the large value of relative time difference between AB and CD phases after distance ~18° could not be matched well. Recent waveform modeling has discovered that lateral velocity variation beneath northeast China and east China is significant as seen from tomographic images (Wang and Niu, 2010; Huang and Zhao, 2006; Li and van der Hilst, 2010). We argue that limitation of earlier data, lateral variation of the MTZ, and subtle effect of variation in physical properties on P and S velocities might contribute to the discrepancy.

5.2. Subduction related high velocity layer

Generally, seismic wave speed in the MTZ mainly reflects variation in thermal or compositional anomaly. P velocity models from Tajima and Grand (1998), Wang and Niu (2010) and Wang and Chen (2009) showed a low gradient high velocity layer at the base of the upper mantle, but with varied thickness. Both P and S wave velocity structures in our study, for the first time, show a quite consistent feature of a high velocity layer with thickness $\sim 140 \pm 20$ km just atop the 660. The velocity gradient increases at depth ~525 km with values of 5.2×10^{-3} km s^{-1} km^{-1} and 4.2×10^{-3} km s^{-1} km^{-1} for P and S waves, respectively. The gradient decreased to a very low value at depth around 600 km, constituting the lower part of the high velocity layer. This feature is robust since triplication for all the three events with different epicentral depths and focal mechanisms shows a consistent feature of a long extension of cusp-B in both P and SH waveforms. We regard that the overall feature of the high velocity layer is in agreement with the tomographic image (e.g. Van der hilst et al., 1991; Huang and Zhao, 2006) in which a stagnant slab lying horizontally in the MTZ, and the thickness of slab trapped in the MTZ is estimated to be ~140 km, which could not be constrained from seismic tomographic images.

The observed P and S velocity anomalies can be converted to a temperature deficit if assuming that the velocity variations are purely of thermal origin. The average P and S velocity anomalies relative to the linear trend of the velocity throughout the MTZ are ~0.8% and 1.1%, respectively, with the maximum value of 1.5% and 2.2% at depth ~600 km. Taking the temperature derivative of -6.0 to -7.8×10^{-5} K^{-1} and -4.1 to -4.5×10^{-5} K^{-1} for S and P velocities (Cammarano et al., 2003) respectively, we can estimate that the observed velocity anomaly corresponds to a ~140–200 K temperature variation.

5.3. A velocity transitional 660-km discontinuity

The velocity transitional 660-km discontinuity, or a "broad 660" beneath northeast China, is first examined in Wang and Niu's work (2010) through a set of regional P waveform investigations. Here both P and SH waveform modeling show a consistent feature of a transitional 660 with thickness $\sim 44 \pm 6$ km, which is 6 km thinner than that of Wang and Niu (2010). This feature is mainly constrained by the emerging distance of cusp-C, which is most sensitive to velocity gradient at the top of the lower mantle. As shown by synthetic waveform modeling, the CD phase will appear at a shorter distance for a sharp discontinuity due to the effective wave refraction (Fig. S1).

The observed velocity transitional 660, which extends from 665 to 709 km is hard to be explained by a solely postspinel transformation. The decomposition of ringwoodite occurs at ~23 GPa in a very

narrow pressure depth interval (Litasov et al., 2005). Addition of little water might shift the phase boundary to higher pressure (Litasov et al., 2006); however, it would not have a significant effect on the pressure interval. It is thus reasonable to speculate, in addition to the postspinel phase transformation, a series of non-olivine phase transformation might contribute to the observed broad 660.

Garnet is one of the major minerals in either pyrolite or piclogite assemblages of the upper mantle. At low mantle temperature, majorite garnet will transform to ilemenite first at the bottom of the MTZ before it starts to transform to perovskite. The majorite–perovskite transition boundary has a positive pressure–temperature slope in contrast to the negative Clapeyron slope of the postspinel phase boundary, and the phase transition in garnet could spread over a depth interval of 660–760 km, depending on mantle composition. Our preferred P and SH velocity structures seem to show that, beneath the old subduction zone, non-olivine phase transition plays an important role in shaping the observed 660. In fact, multi-660-km-discontinuity structure is identified very close to our studied region through various P-to-S scattered receiver function analyses (e.g. Niu and Kawakatsu, 1996; Ai et al., 2003).

5.4. Low shear velocity: a water-bearing mantle transition zone

The most remarkable feature of the velocity models obtained from the same station-event geometry of P and S waves is the presence of a MTZ with low shear velocity relative to a normal P wave velocity. The observed large relative time between AB and CD phases in transversal seismograms after distance $\sim 18^\circ$ for all the three deep events and S–P travel time residuals analysis all require a slow shear velocity in the MTZ. It is generally regarded that increased temperature is likely to reduce seismic wave speed and vice versa. Since it affects both bulk and shear moduli of the rock, pure thermal effects could not explain the observed discordance between variations in V_p and V_s.

Major elements, e.g. Mg and Fe, might affect velocity also. Effects of Fe content on elastic moduli are conducted using different techniques, e.g. ultrasonic measurements (Higo et al. 2006) and Brillouin scattering (Sinogeikin et al., 2001). There is some inconsistency in their experiments; however, all results show that with increasing Fe content, or equivalently with decreasing Mg#, both V_p and V_s decrease significantly. Moreover, according to the experimental study by Sinogeikin et al. (1998), a change of 10 mol% Fe content will result in the shear velocity change of 210 m/s, 200 m/s and 90 m/s to olivine, wadsleyite and ringwoodite, respectively. Thus a large variation in Fe content is required to explain the observed 100–200 m/s S velocity anomaly (Jacobsen et al., 2004; Jacobsen and Smyth, 2006).

Water is one of the most abundant volatile components on Earth's surface, and can be supplied to the deep mantle by subducting slabs (e.g. Irifune et al., 1998). Presence of little water is believed to have a remarkable ability to affect rheological property of mantle minerals. It has been estimated that the dominant upper mantle minerals, olivine and its high-pressure polymorphs can store water up to 3 wt% in their crystal structures. Recently, lots of efforts have been made to estimate the absolute water content in the mantle beneath northwestern Pacific subduction zones. Geophysical observations of electrical conductivity measurement beneath northeast China discover a high value at depth around MTZ (Ichiki et al., 2006; Karato, 2011; Huang et al., 2005). Geochemical analysis of Cenozoic intraplate basalts around Changbai volcano (Fig. 1) suggests an intensive hydration of the MTZ which might be caused by an ancient slab stagnation (Kuritani et al., 2011).

Seismological observations of velocity, and especially the Poisson ratio, are believed to be quite useful in inferring water content. We estimated the V_p/V_s ratio of the upper MTZ and the anomalously fast lower part to be ~ 1.89 and ~ 1.86, respectively, which are 2.7% and 2.1% higher than values of 1.84 and 1.82 in the global average model iasp91. Experiments by Jacobsen and Smyth (2006) show that P-velocities of hydrous Fo90-ringwoodite are indistinguishable from anhydrous Fo90-ringwoodite at the condition of lower MTZ, while the shear wave velocity remains 1–2% slower than anhydrous Fo90-ringwoodite at MTZ pressures, which suggests that the elevated V_p/V_s ratio is a characteristic feature of hydration in the MTZ. It is thus reasonable to assume the presence of hydroxyls that structurally incorporate into mantle minerals beneath study region (Jacobsen and Smyth, 2006; Jacobsen et al., 2004). Laboratory experiment on Fe-bearing ringwoodite indicates that adding 0.1 wt% H_2O can reduce S-wave velocity by about 40 m/s at lower MTZ condition (Jacobsen et al., 2004). The velocity data for hydrous wadsleyite is limited under higher pressure; however, the same effect of H_2O on V_p, V_s and V_p/V_s is expected in the upper part of the MTZ (Jacobsen and Smyth, 2006). Based on those findings and the V_s reduction of 0.09–0.16 km/s in our shear velocity model, we propose that a possible water content of $\sim$0.2–0.4 wt% ($(3.0–6.0)\times 10^4$ ppm H/Si) exists in the MTZ, which is much higher than the average value of the upper mantle (100–500 ppm H/Si). Our estimation is based on a simple assumption of a unified H_2O distribution through the MTZ, and thus might be a little smaller than the true value considering the highest hydrogen solubility of

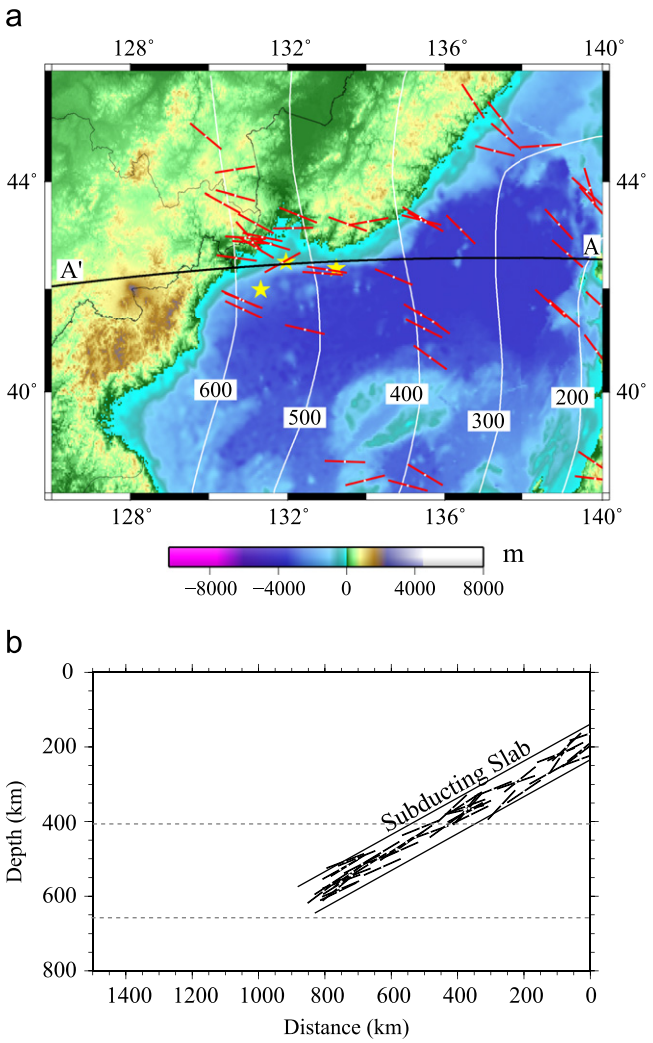

Fig. 7. Distribution of compressive axis of intermediate or deep earthquakes beneath Japan Sea and northeast China. The profile is cut roughly perpendicular to the Waditi–Benioff curve along latitude 43°: (a) plane view and (b) vertical cross section along line A–A′.

wadsleyite (Inoue et al., 2010). Huang et al. (2005) estimated from electric conductivity observation that water content in the MTZ beneath northeast China is around 0.1–0.3 wt%, which is quite consistent with our seismological estimation. Nevertheless, how water is transported and stored in the MTZ is still a question. The phase-B or phase-D decomposition of an ancient stagnant slab might be the source of water (Kuritani et al., 2011; Zhao et al., 2009).

5.5. Implication for stagnation of subducting Pacific slab

It has long been assumed that positive thermal buoyancy associated with the postspinel phase transition plays an important role in preventing slab penetration into the lower mantle. Numerical simulation of mantle convection showed that a two-layered convection can be realized provided that there is a large absolute value of Clapeyron slope (Christensen and Yuen, 1984). Recent high pressure and high temperature experiments, however, suggest that the Clapeyron slope for the postspinel transformation in anhydrous pyrolite is gentle with a value of -1 MPa/K, instead of the previously estimated range of -2 to -3 MPa/K (e.g. Katsura et al., 2003; Fei et al., 2004). With the addition of water, this value becomes more controversial (e.g. Litasov et al., 2005), and the Clapeyron slope is even proposed to be positive. In Fig. 7, we estimated the stress distribution along the slab using the CMT focal mechanism solutions of intermediate-depth and deep earthquakes that occurred after year 1990. The result clearly shows that beneath the Japan trench, the compressional stress axes of almost all deep earthquakes are parallel or sub-parallel to the down-dip motion of the slab, indicating a compression dominated regime in the subducting slab, which has also been suggested by Zhao et al. (2011). Experimental study on the grain growth of ringwoodite (Yamazaki et al., 2005) indicated that ringwoodite in a cold subducting slab has fine grain size and deforms dominantly by diffusion creep with a rather low value of viscosity. Based on our deduction of a water-bearing MTZ from the combined study of S and P waveform modeling, we argued that the strong resistance caused by the large viscosity of the lower mantle acted on the slab resulted in the strong compressional stress. The rheological weakened slab is easily bent and deformed above the 660, and formed a kind of viscosity-dominated stagnation.

To obtain a complete picture of the slab behavior around the 660, we compiled previous studies on topography of the 660 beneath northeast China. The white dashed line in Fig. 1 marks the profile where undulation of the 660 is mapped in detail by the source-sided S-to-P converted waves (Li et al. 2008). To the east of the profile where the subducting slab has not reached the discontinuity, the 660 is almost flat, while it changed sharply west of $\sim$131°E, with a maximum depression of 20 km reported at the west end of the studied sampling point (Figs. 1 and 8). Further west, a maximum of 30–35 km depression was mapped just to the northeast corner of our study region (orange shadow in Fig. 1) using receiver function technique. We thus attain a more clear and consistent image of the behavior of the subducting Pacific slab beneath Japan trench. We divide the subducting slab into three parts: downgoing, bottoming and stagnant parts. During the downgoing part, no change of the 660-km discontinuity occurred since there is no interaction between the slab and the boundary. When the slab encountered the 660 around $\sim$131°E, the 660 deflected sharply due to the coldness of the slab, with the largest depression corresponding to the coldest core of the slab, and then formed the bottoming part. Due to the large viscosity contrast between the slab and lower mantle, the slab bent, extended westward and stayed stagnant in the MTZ.

A slab with thickness $\sim$80–90 km has been mapped through seismic tomographic images, which is quite consistent with an estimation of a 120 Ma year old slab. The thickness of the high velocity layer in the stagnant part, however, could not be constrained well through tomographic technique, and the high velocity anomaly seems to distribute throughout the whole MTZ (Huang and Zhao, 2006; Li and van der Hilst, 2010). Our result suggested that the stagnant slab has a thickness $\sim$140 km, which seems to be 50–60 km thickened from the initial value. We argue that the large viscosity contrast between the lower and upper mantles results in the obvious thickening of slab in the stagnant part. Numerical experiments of mantle convection (Kameyama and Nishioka, 2012) show that thickening of the slab will occur near the oceanward end of stagnant slabs where they meet the 660 and bend, and it will be significant for a larger viscosity contrast and trench retreat velocity. The retreat of trench under Japan–Kurile arc from Miocene (Miller et al., 2006) revealed by Paleotectonic reconstruction studies might also facilitate the thickening of the slab.

Combined with tomographic images beneath northeast China, our results imply that the stagnant Pacific slab lies subhorizontally in a water-bearing MTZ beneath northeast China (Fig. 8). Geochemical analysis of a limit basalt samples around Changbai volcano has revealed a regional water-rich MTZ (Kuritani et al., 2011). From the distribution of turning points of CD phase (white points in Fig. 1 with distance $<25^{\circ}$), which is most critical in constraining discrepancy structure between V_p and V_s, we argue that the hydrous MTZ is more widely distributed than previous

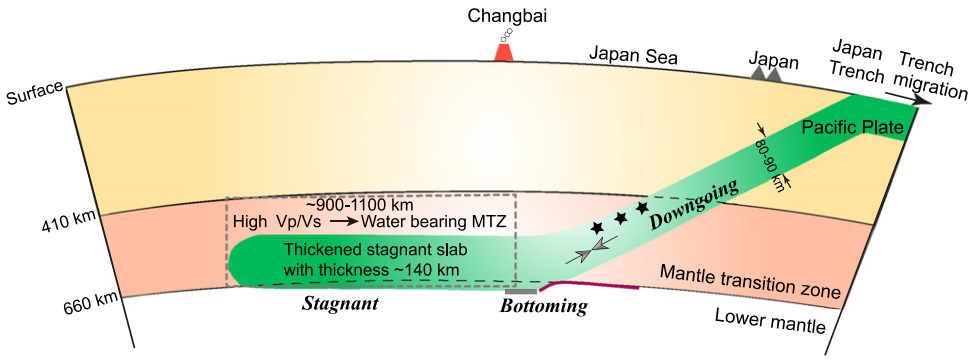

Fig. 8. A schematic map showing major features of the upper mantle structure and the subducting Pacific slab inferred from simultaneously P and SH waveform modeling. The slab can be divided into downgoing, bottoming and stagnant parts. The bottoming part corresponds to the region where a depression $\sim$30 km of the 660 is mapped (Li and Yuan, 2003). The purple line indicates the undulation of the 660 mapped by S-to-P converted waves (Li et al., 2008) along a profile (Fig. 1), which connects the downgoing and bottoming parts of the slab. The gray arrow marks the compressional stress obtained from focal mechanism solutions. The dark gray rectangle roughly corresponds to the region with overall low V_s and high V_p/V_s ratio, indicating a water-bearing MTZ, which might extend 900–1100 km westward of Changbai volcano. The stagnant slab is thickened to 140 km due to the large resistance acted on the slab. Stars roughly indicate the location of deep earthquakes. (For interpretation of the references to color in this figure legend, the reader is referred to the web version of this article.)

geochemical deduction. It might extend as far as 118°E, roughly corresponding to the steepest topographic gradient belt in China.

6. Conclusions

We have shown that fine-scale seismic structure in the heterogeneous MTZ can be obtained effectively from triplication waveform modeling for a set of densely distributed stations. Simultaneous modeling of S and P waveforms provides a useful way for identifying thermal or compositional anomalies associated with subduction process. A high velocity layer with thickness ~140 km is detected lying in the MTZ which corresponds to the deflected and stagnant Pacific slab. The high V_p/V_s ratio in the MTZ indicates a water-bearing MTZ, which might extend 900–1100 km westward of Changbai volcano. Our results support the scenario that due to the large resistance exerted by the lower mantle, the rheology weakened slab bends easily while encountering the 660 and then lies subhorizontally in the water-rich MTZ. Nevertheless, finite difference waveform synthetic for a 3D velocity structure should be applied to account for the lateral velocity variation, and simulation on the interaction between the 660 and the subducting slab is required for a full understanding of the geodynamic mechanism and composition of the upper mantle beneath the northwestern Pacific subduction zone.

Acknowledgments

This research is supported by NSFC (J. Li, Grant 41074034). We thank Risheng Chu and an anonymous referee for constructive and valuable comments, which improved the manuscript greatly. Thanks to Dr. Shengqiang Li of China Earthquake Administration for providing the focal mechanism solution for event 20081022 with Mw 4.7. Lingling Ye has joined the discussion and contributed to earlier work. Thanks to Prof. Fenglin Niu's discussion on travel time analysis and seismic structure beneath northeast China. We thank the Data Management Centre of China National Seismic Network at Institute of Geophysics, China Earthquake Administration and IRIS DMS, for providing seismic data. Sac2000 and GMT are used in basic data processing and plotting of some figures.

Appendix A. Supplementary materials

Supplementary data associated with this article can be found in the online version at http://dx.doi.org/10.1016/j.epsl.2013.02.026.

References

Ai, Y., Zheng, T., Xu, W., Dong, D., 2003. A complex 660 km discontinuity beneath northeast China. Earth Planet. Sci. Lett. 212, 63–71.
Bijwaard, H., Spakman, W., Engdahl, E., 1998. Closing the gap between regional and global travel time tomography. J. Geophys. Res. 103, 30055–30078.
Brudzinski, M.R., Chen, W.P., 2000. Variations in P wave speeds and outboard earthquakes: evidence for a petroligic anomaly in the mantle transition zone. J. Geophys. Res. 105, 21661–21682.
Brudzinski, M.R., Chen, W.-P., 2003. A petrologic anomaly accompanying outboard earthquakes beneath Fiji-Tonga: corresponding evidence from broadband P and S waveforms. J. Geophys. Res., 108, 2299, http://dx.doi.org/10.1029/2002JB002012.
Buland, R., Chapman, C.H., 1983. The computation of seismic travel times. Bull. Seismol. Soc. Am. 73, 1271–1302.
Cammarano, F., Goes, S., Vacher, P., Giardini, D., 2003. Inferring upper-mantle temperatures from seismic velocities. Phys. Earth Planet. Inter. 138, 197–222.
Christensen, U.R., Yuen, D.A., 1984. The interaction of a subducting lithospheric slab with a chemical or phase boundary. J. Geophys. Res. 89, 4389–4402.
de Wit, R.W.L., Trampert, J., van der Hilst, R.D., 2012. Toward quantifying uncertainty in travel time tomography using the null-space shuttle. J. Geophys. Res. 117, B03301.
Fei, Y., Van Orman, J., Li, J., van Westrenen, W., Sanloup, C., Minarik, W., Hirose, K., Komabayashi, T., Walter, M., Funakoshi, K., 2004. Experimentally determined postspinel transformation boundary in Mg_2SiO_4 using MgO as an internal pressure standard and its geophysical implications. J. Geophys. Res. 109, B02305.
Fukao, Y., 1977. Upper mantle P structure on the ocean side of the Japan-Kurile arc. Geophys. J. Int. 50, 621–642.
Fukao, Y., Widiyatoro, S., Obayashi, M., 2001. Stagnant slabs in the upper and lower mantle transition region. Rev. Geophys. 39, 291–323.
Fukao, Y., Obayashi, M., Nakakuki, T., 2009. Stagnant slab: a review. Annu. Rev. Earth Planet. Sci. 37, 19–46.
Gorbatov, A., Kennett, B.L.N., 2003. Joint bulk-sound and shear tomography for Western Pacific subduction zones. Earth Planet. Sci. Lett. 210, 527–543.
Grand, S.P., Helmberger, D.V., 1984. Upper mantle shear structure of North America. Geophys. J. R. Astron. Soc. 76, 399–438.
Higo, Y., Inoue, T., Li, B., Irifune, T., Liebermann, R.C., 2006. The effect of iron on the elastic properties of ringwoodite at high pressure. Phys. Earth Planet. Inter. 159, 276–285.
Huang, J.L., Zhao, D.P., 2006. High-resolution mantle tomography of China and surrounding regions. J. Geophys. Res. 111, B09305.
Huang, X., Bai, W., Xu, Y.S., Karato, S.-i., 2005. Influence of hydrogen on electrical conductivity of wadsleyite and ringwoodite with its geodynamics implications. Acta Petrol. Sin. 21 (6), 1743–1748 (in Chinese).
Ichiki, M., Baba, K., Obayashi, M., Utada, H., 2006. Water content and geotherm in the upper mantle above the stagnant slab: interpretation of electrical conductivity and seismic P-wave velocity models. Phys. Earth Planet. Inter. 155, 1–15.
Inoue, T., Wada, T., Sasaki, R., Yurimoto, H., 2010. Water partitioning in the earth's mantle. Phys. Earth Planet. Inter. 183, 245–251.
Irifune, T., Kubo, N., Isshiki, M., Yamasaki, Y., 1998. Phase transformations in serpentine and transportation of water into the lower mantle. Geophys. Res. Lett. 25, 203–206.
Ito, E., Takahashi, E., 1989. Postspinel transformations in the system Mg_2SiO_4–Fe_2SiO_4 and some geophysical implications. J. Geophys. Res. 94, 10637–10646.
Jacobsen, S., Smyth, J., 2006. Effect of water on the sound velocities of ringwoodite in the transition zone. Geophys. Monogr.—Am. Geophys. Union 168, 131.
Jacobsen, S.D., Smyth, J.R., Spetzler, H., Holl, C.M., Frost, D.J., 2004. Sound velocities and elastic constants of iron-bearing hydrous ringwoodite. Phys. Earth Planet. Inter. 143–144, 47–56.
Kameyama, M., Nishioka, R., 2012. Generation of ascending flows in the Big Mantle Wedge (BMW) beneath northeast Asia induced by retreat and stagnation of subducted slab. Geophys. Res. Lett. 39, L10309.
Karato, S.-i., 2011. Water distribution across the mantle transition zone and its implications for global material circulation. Earth Planet. Sci. Lett. 301, 413–423.
Karato, S.-i., Karki, B., 2001. Origin of lateral variation of seismic wave velocities and density in the deep mantle. J. Geophys. Res. 106 (21), 771–21784.
Katsura, T., Yamada, H., Shinmei, T., Kubo, A., Ono, S., Kanzaki, M., Yoneda, A., Walter, M.J., Ito, E., Urakawa, S., Funakoshi, K., Utsumi, W., 2003. Post-spinel transition in Mg_2SiO_4 determined by high P–T in situ X-ray diffractometry. Phys. Earth Planet. Inter. 136, 11–24.
Kuritani, T., Ohtani, E., Kimura, J.-I., 2011. Intensive hydration of the mantle transition zone beneath China caused by ancient slab stagnation. Nat. Geosci. 4, 713–716.
Li, C., van der Hilst, R.D., 2010. Structure of the upper mantle and transition zone beneath Southeast Asia from traveltime tomography. J. Geophys. Res. 115, B07308.
Li, J., Chen, Q.F., Vanacore, E., Niu, F.L., 2008. Topography of the 660-km discontinuity beneath northeast China: implications for a retrograde motion of the subducting Pacific slab. Geophys. Res. Lett. 35, L01302.
Li, J., Niu, F., 2010. Seismic anisotropy and mantle flow beneath northeast China inferred from regional seismic networks. J. Geophys. Res. 115, B12327.
Li, S.Q., 2012. Quasi-Automatic Waveform Inversion of Focal Mechanisms of Moderate and Small Earthquakes on High-Performance Cluster Computing System and Applications. PhD. Thesis (in Chinese).
Li, X.Q., Yuan, X.H., 2003. Receiver functions in northeast China—implications for slab penetration into the lower mantle in northwest Pacific subduction zone. Earth Planet. Sci. Lett. 216, 679–691.
Litasov, K.D., Ohtani, E., Sano, A., 2006. Influence of water on major phase transitions in the Earth's mantle, Earth's Deep Water Cycle. AGU, Washington, DC, pp. 95–111.
Litasov, K.D., Ohtani, E., Sano, A., Suzuki, A., Funakoshi, K., 2005. Wet subduction versus cold subduction. Geophys. Res. Lett. 32, L13312.
Miller, M.S., Kennett, B.L.N., Toy, V.G., 2006. Spatial and temporal evolution of the subducting Pacific plate structure along the western Pacific margin. J. Geophys. Res. 111, B02401.
Molnar, P., Chen, W.-P., 1984. S–P wave travel time residuals and lateral inhomogeneity in the mantle beneath Tibet and the Himalaya. J. Geophys. Res. 89, 6911–6917.
Niu, F., Kawakatsu, H., 1996. Complex structure of mantle discontinuities at the tip of the subducting slab beneath northeast China. J. Phys. Earth 44, 701–711.
Niu, F., Li, J., 2011. Component azimuths of the CEArray stations estimated from P-wave particle motion. Earthquake Sci. 24, 3–13.
Pei, S., Zhao, J., Sun, Y., Xu, Z., et al., 2007. Upper mantle seismic velocities and anisotropy in China determined through Pn and Sn tomography. J. Geophys. Res. 112, B05312.
Sinogeikin, S., Katsura, T., Bass, J., 1998. Sound velocities and elastic properties of Fe-bearing wadsleyite and ringwoodite. J. Geophys. Res. 103, 20819–20825.

Sinogeikin, S.V., Bass, J.D., Katsura, T., 2001. Single-crystal elasticity of γ-$(Mg_{0.91}Fe_{0.09})_2SiO_4$ to high pressures and to high temperatures. Geophys. Res. Lett. 28, 4335–4338.
Song, A.T.-R., Helmberger, D.V., Grand, S.P., 2004. Low-velocity zone atop the 410-km seismic discontinuity in the northwestern United States. Nature 427, 530–533.
Tajima, F., Grand, S.P., 1995. Evidence of high-velocity anomalies in the transition zone associated with Southern Kurile subduction zone. Geophys. Res. Lett. 22, 3139–3142.
Tajima, F., Grand, S.P., 1998. Variation of transition zone high-velocity anomalies and depression of 660 km discontinuity associated with subduction zones from the southern Kuriles to Izu-Bonin and Ryukyu. J. Geophys. Res. 103, 15015–15036.
Tajima, F., Katayama, I., Nakagawa, T., 2009. Variable seismic structure near the 660 km discontinuity associated with stagnant slabs and geochemical implications. Phys. Earth Planet. Inter. 172, 183–198.
Tajima, F., Nakagawa, T., 2006. Implications of seismic waveforms: complex physical properties associated with stagnant slab. Geophys Res Lett 33, L03311.
Van der hilst, R., Engdahl, R., Spakman, W., Nolet, G., 1991. Tomographic imaging of subducted lithosphere below Northwest Pacific Island arcs. Nature 353, 37–43.
Wang, B., Niu, F., 2010. A broad 660-km discontinuity beneath northeastern China revealed by dense regional seismic networks in China. J. Geophys. Res. 115, B06308.
Wang, K., Yao, Z., 1991. Upper mantle P velocity structure of southern China. Chin. J. Geophys. 34, 309–317 (in Chinese).
Wang, T., Chen, L., 2009. Distinct velocity variations around the base of the upper mantle beneath northeast Asia. Phys. Earth Planet. Inter. 172, 241–256.
Wang, Y., Wen, L.X., Weidner, D., He, Y.M., 2006. SH velocity and compositional models near the 660-km discontinuity beneath South America and northeast Asia. J. Geophys. Res. 111, B07305.
Yamazaki, D., Inoue, T., Okamoto, M., Irifune, T., 2005. Grain growth kinetics of ringwoodite and its implication for rheology of the subducting slab. Earth Planet. Sci. Lett. 236, 871–881.
Ye, L., Li, J., Tseng, T.-L., Yao, Z., 2011. A stagnant slab in a water-bearing mantle transition zone beneath northeast China: implications from regional SH waveform modelling. Geophys. J. Int. 186, 706–710.
Zhao, D., Tian, Y., Lei, J., Liu, L., Zheng, S., 2009. Seismic image and origin of the Changbai intraplate volcano in East Asia: role of big mantle wedge above the stagnant Pacific slab. Phys. Earth Planet. Inter. 173, 197–206.
Zhao, D., Yu, S., Ohtani, E., 2011. East Asia: seismotectonics, magmatism and mantle dynamics. J. Asian Earth Sci. 40, 689–709.
Zheng, X.-F., Yao, Z.-X., Liang, J.-H., Zheng, J., 2010. The role played and opportunities provided by IGP DMC of China National Seismic Network in Wenchuan Earthquake Disaster Relief and Researches. Bull. Seismol. Soc. Am. 100, 2866–2872.
Zhu, L., Helmberger, D., 1996. Advancement in source estimation techniques using broadband regional seismograms. Bull. Seismol. Soc. Am. 86, 1634–1641.